



THE UNIVERSITY *of* EDINBURGH

Edinburgh Research Explorer

One-pot hydrothermal synthesis of magnetic N-doped sludge biochar for efficient removal of tetracycline from various environmental waters

Citation for published version:

Ma, Y, Lu, T, Tang, J, Li, P, Mašek, O, Yang, L, Wu, L, He, L, Ding, Y, Gao, F, Qi, X & Zhang, Z 2022, 'One-pot hydrothermal synthesis of magnetic N-doped sludge biochar for efficient removal of tetracycline from various environmental waters', *Separation and Purification Technology*.
<https://doi.org/10.1016/j.seppur.2022.121426>

Digital Object Identifier (DOI):

[10.1016/j.seppur.2022.121426](https://doi.org/10.1016/j.seppur.2022.121426)

Link:

[Link to publication record in Edinburgh Research Explorer](#)

Document Version:

Peer reviewed version

Published In:

Separation and Purification Technology

General rights

Copyright for the publications made accessible via the Edinburgh Research Explorer is retained by the author(s) and / or other copyright owners and it is a condition of accessing these publications that users recognise and abide by the legal requirements associated with these rights.

Take down policy

The University of Edinburgh has made every reasonable effort to ensure that Edinburgh Research Explorer content complies with UK legislation. If you believe that the public display of this file breaches copyright please contact openaccess@ed.ac.uk providing details, and we will remove access to the work immediately and investigate your claim.



1 **One-pot hydrothermal synthesis of magnetic N-doped sludge**
2 **biochar for efficient removal of tetracycline from various**
3 **environmental waters**

4 Yongfei Ma^a, Tingmei Lu^a, Jiayi Tang^a, Ping Li^b, Ondřej Mašek^c, Lie Yang^a, Li Wu^a, Liuyang He^a,

5 Yongzhen Ding^d, Feng Gao^b, Xuebin Qi^b, Zulin Zhang^{a, e*}

6 *^a School of Resources and Environmental Engineering, Wuhan University of Technology, Wuhan*

7 *430070, China*

8 *^b China-UK Water and Soil Resources Sustainable Utilization Joint Research Centre, Farmland*

9 *Irrigation Research Institute, Chinese Academy of Agricultural Sciences, Xinxiang 453002, China*

10 *^c UK Biochar Research Centre, School of GeoSciences, University of Edinburgh, Alexander Crum*

11 *Brown Road, Crew Building, EH9 3FF, Edinburgh, UK*

12 *^d Agro-Environmental Protection Institute, Ministry of Agriculture and Rural Affairs, Tianjin 300191,*

13 *China*

14 *^e The James Hutton Institute, Craigiebuckler, Aberdeen AB15 8QH, UK*

15
16
17
18
19
20
21 _____
22 * **Corresponding authors:** Zulin.Zhang@hutton.ac.uk (Zulin Zhang).

24 **Abstract:** Efficient removal of zwitterionic tetracycline (TC) from water is a critical
25 environmental challenge which is not fully addressed by conventional treatment technologies. A
26 magnetic N-doped sludge biochar (MNSBC) was the first time synthesized by a simple one-pot
27 hydrothermal method. The maximum adsorption capacity of MNSBC for TC was 197.3 mg/g at
28 298 K. Solution pH, ionic species/strength and humic acid concentration were the critical factors
29 affecting TC adsorption by MNSBC. Elovich and Freundlich models better describing the
30 experimental data illustrated that TC adsorption onto MNSBC was a multi-layer physicochemical
31 adsorption process. Lewis acid-base, π - π conjugation, electrostatic interactions and pore filling
32 were the main adsorption mechanisms. MNSBC also exhibited excellent adsorption performance
33 for TC in various environmental waters, which achieved removal rates of up to 91.6%, 89.0%,
34 82.0% and 80.8% in mineral, tap, lake and river waters, respectively. The magnetic susceptibility
35 of MNSBC allowed it to be easily collected after adsorption. Regeneration using NaOH could
36 maintain its sustainable adsorption performance. Furthermore, MNSBC showed a very low release
37 levels of iron and total nitrogen at all pH ranges (from 3 to 11), which suggested its suitability for
38 water treatment applications. This study developed a simple technology for synthesis of effective
39 TC adsorbent for different environmental waters and identified a circular economy pathway to
40 reuse of water industry wastes.

41 **Keywords:** Sludge; biochar; Hydrothermal synthesis; Tetracycline; Adsorption mechanisms

42

43 **1. Introduction**

44 Various antibiotics including tetracyclines, fluoroquinolones, macrolides, β -lactams,
45 sulfonamides and chloramphenicols had been widely used to prevent and treat diseases [1]. China
46 had overtaken the United States as the world's greatest consumer of antibiotics with annual use of
47 antibiotics exceeding 1.62×10^5 tons. 52% of this amount was used in animal husbandry for
48 improving their growth rate [2]. This led to a discharge of a large amount of unmetabolized
49 antibiotics into the environment via feces and urine which caused serious antibiotics pollution of
50 aquatic ecosystems with potential risks to human health [3]. Tetracycline (TC) was the most
51 widely used veterinary antibiotic, and was one of the most frequently detected antibiotics with the
52 high concentration in natural waters [4]. Efficient removal of TC from water is an urgent problem
53 because removal efficiency of the traditional wastewater treatment technologies is insufficient [5].

54 Adsorption [6], constructed wetlands [7], advanced oxidation [8] and bioremediation [9] have
55 been studied to eliminate antibiotics from waters. Among these technologies, adsorption had
56 shown numerous benefits, such as cost-effectiveness, simple operation and minimal byproducts
57 generation. The selection of adsorbent was crucial for effective removal of TC. Varieties of
58 adsorbents including biochar [10], carbon nanotubes [11], graphene oxide [12], and clay minerals
59 [13] had been used to adsorb TC. Biochar was mainly produced from biomass wastes (e.g., rice
60 straw and sawdust) [14,15] under oxygen-limited atmosphere, and the superior physicochemical
61 properties guaranteed its promising adsorption capacity for TC. In addition to these biomass
62 resources, there were large amounts of municipal sludge generated at wastewater treatment plants
63 (WWTPs) due to rapid population growth and urbanization [16]. The production of municipal
64 sewage sludge in China had reached 6.0×10^7 t in 2020 and kept rising. The cost of sludge

65 management shared about 20-60% of the total running costs of WWTPs [17]. Traditional sludge
66 disposal techniques, such as land filling and incineration might cause groundwater and air
67 pollution, respectively. However, the high organic matter content of municipal sludge enabled it to
68 be an ideal raw material for biochar production [18]. Using sludge biochar (SBC) as the adsorbent
69 to adsorb antibiotics could simultaneously realize resource recovery of byproducts in WWTPs as
70 well as effective removal of antibiotics. Previous studies showed that SBC performed a relatively
71 weak adsorption capacity due to its poor physicochemical characteristics [18,19]. The adsorption
72 capacity of biochar mainly depended on its surface area, pore volume and functional groups [20].
73 Many technologies (e.g., carbon nanotubes, KOH, ZnCl₂ and N-doped modification) have been
74 developed to improve these characteristics of biochar for the better adsorption performance
75 [1,21-23]. The application of carbon nanotubes, KOH, ZnCl₂ modifications were limited due to
76 the high cost/toxic impact on organisms, toxic CO generation/high pyrolysis temperature and
77 potential heavy metal release risk, respectively. While N-doping was identified as a promising
78 technique due to the similar size of N and C atoms, which enabled it to easily permeate into the
79 carbon lattice structure of biochar and changed its electron distribution because of the one more
80 outermost electron in N compared to that of C [22]. Also, it could introduce N-containing
81 functional groups which would change biochar structure and surface chemistry [24]. Additionally,
82 the advantages of low cost, no heavy metal/toxic gas release risks enabled it to be a promising
83 technology to modify biochar for its physicochemical properties enhancement. Urea (CO(NH₂)₂)
84 was regarded as an ideal N-doping reagent because of its low price and high N content (46.7%),
85 and it had been extensively used to modify biochar for porous composite material production [25].
86 However, in most cases this approach required impregnation or secondary pyrolysis, which made

87 the process more complex and costly, and achieved only poor activation efficiencies due to the
88 diffusion resistance during impregnation. Hydrothermal process was operated at a closed
89 autoclave using water as the reaction media under moderate temperature (180-280°C) and
90 self-pressure which was considered as a cost-effective method to enhance the physicochemical
91 properties of biochar [26]. To the best of our knowledge, hydrothermal method has not been used
92 to modify biochar by N-doping. In our previous works, we proved that using $\text{ZnCl}_2/\text{FeCl}_3$ or KOH
93 combined with $\text{MgCl}_2/\text{FeCl}_3$ hydrothermal activation could significantly enhance the adsorption
94 performance of SBC [27,28]. In addition to enhance the adsorption performance of biochar by
95 increasing the porous structure of biochar (through hindering the shrinkage of carbon matrix) and
96 Fe-O complexation of FeCl_3 modification, it could also introduce magnetic component Fe_3O_4 on
97 biochar surface which provided a workable approach for solid-liquid separation, also this was
98 beneficial for biochar regeneration and reuse in cyclic experiments [29,30]. Herein, $\text{CO}(\text{NH}_2)_2$ and
99 FeCl_3 were the first time used to modify SBC by one-pot hydrothermal activation and used to
100 adsorptive removal of TC from water. To obtain its practical application, TC was added into
101 various types of water to investigate its adsorption performance, and its environmental safety and
102 regeneration were also evaluated in this study.

103 The main objectives of this study were to: (1) synthesize a $\text{CO}(\text{NH}_2)_2$ and FeCl_3 co-modified
104 SBC (MNSBC) by one-pot hydrothermal method for TC adsorptive removal; (2) investigate the
105 dominant mechanisms of TC adsorption onto MMSBC by model fitting, environmental factors
106 experiments and physicochemical characterization analysis; (3) study the adsorption performance
107 of MNSBC for TC in various actual waters (mineral, tap, lake and river waters); (4) assess the
108 environmental safety (Fe and N dissolution) and sustainable adsorption performance of MNSBC

109 synthesized in this study.

110 **2. Materials and methods**

111 *2.1 SBC and MNSBC preparation*

112 All used materials were given in Text S1.

113 Municipal sludge was dried at 343 K, then it was transported into the tube furnace
114 (BTF1200C, Best Equipment, Hefei, China) for pyrolysis at 673, 773, 873 and 973 K with the
115 heating rate of 10°C/min under nitrogen atmosphere, and holding time of 120 min. At the end, the
116 produced biochars were cooled to room temperature, and these samples were labeled as SBC-673,
117 SBC-773, SBC-873 and SBC-973, respectively. N-doping was done by adding 5.0 g SBC-873 (the
118 reason for using SBC-873 as the precursor had been confirmed in the section of 3.2 (Fig. 4(a)),
119 and it would be called SBC in the following text) into the solution (60 mL) containing 2.5 g, 5.0 g
120 and 10.0 g CO(NH₂)₂, respectively, then they were stirred with a magnetic stirrer at 500 r/min for
121 60 min. Immediately after that, the mixed solutions were transported into the hydrothermal
122 reactors and underwent continuous hydrothermal activation for 720 min at temperature of 493 K.
123 The activated samples were washed three times with deionized water, then they were dried,
124 grinded and sieved (0.15 mm), and labeled as NSBC-0.5, NSBC-1 and NSBC-2. The preparation
125 of MSBC and MNSBC were using FeCl₃·6H₂O (5.0 g) and FeCl₃·6H₂O (5.0 g)/CO(NH₂)₂ (5.0 g)
126 (the dose of CO(NH₂)₂ used here had been confirmed in the section of 3.2) as the modifiers,
127 respectively, and the other operations were the same as those of NSBC-1 (NSBC).

128 *2.2 Batch adsorption experiments*

129 Batch experiments were employed to investigate the adsorption characteristics and
130 mechanisms of TC adsorption onto biochar. Kinetics, isotherms and thermodynamics experiments

131 were conducted to study the adsorption process. Also, the environmental safety as well as
132 regeneration performance of biochar were evaluated in this study. Finally, the TC removal
133 efficiency in various real water samples (mineral, tap, lake and river waters) by MNSBC was
134 investigated. The concentration of TC was measured by ultraviolet spectrophotometry (UV-1500C,
135 Macy China Instruments Inc., Shanghai, China) at the wavelength of 360 nm. All the conditions of
136 experiments were given at the bottom of figures.

137 Biochar characteristics were provided in Text S2.

138 **3. Results and discussions**

139 *3.1 Characterization*

140 The crystal structures of biochars were presented in Fig. 1(a). The characteristic diffraction
141 peaks around $2\theta=20^\circ$ were identified as the amorphous carbons. The diffraction peaks located at
142 36.5° (110), 39.5° (102), 50.1° (112), 59.9° (121) and 68.3° (122) proved the presence of SiO_2
143 (JCPDS No.99-0088). The diffraction peaks at $2\theta=26.3^\circ$ corresponded to the graphite crystals [31].
144 As expected, the graphitization degree of biochar increased with the pyrolysis temperature, also
145 FeCl_3 and $\text{CO}(\text{NH}_2)_2$ single or co-modification enhanced this characteristic. This was desirable for
146 TC adsorption as π - π conjugation generated between the graphitic structure of biochar and
147 aromatic rings of TC [32]. The diffraction peaks of $2\theta=30.1^\circ$ (220), 35.4° (311), 42.9° (400) and
148 62.4° (440) on MSBC and MNSBC were due to the presence of magnetic Fe_3O_4 (JCPDS
149 No.19-0629) [33]. The saturation magnetization value of MNSBC was 9.59 emu/mg (Fig. 1(e)).
150 The great magnetic strength of MNSBC allowed it to be quickly collected after adsorption using a
151 magnet.

152 The porous structure of biochars before and after modification were determined by BET. The

153 N₂ adsorption/desorption curves of all biochars were typical IV curves with H₃ hysteresis loops
154 (the slopes showed a significant increasing at $P/P_0=0.5-0.8$) (Fig. 1(c)), which illustrated mesopores
155 or macropores were generated on biochars [34]. The pore diameter distribution listed in Fig. 1(d)
156 showed that the biochars of SBC-673, SBC-773, SBC and SBC-973 exhibited two pore size
157 characteristics of 3.56 nm and 15.3 nm, and the pore diameter of MSBC, NSBC and MNSBC
158 around 3.64 nm. It was well accepted that the adsorbent would perform the maximal adsorption
159 capacity when the pore diameter of biochar was 1.7-3.0 times that of adsorbate [35]. The pore
160 diameter of MNSBC were mainly concentrated around 3.56 nm, which was 2.89 times of TC
161 molecule size (1.23×0.84×0.67 nm). This pore size characteristic facilitated the rapid and efficient
162 adsorption of TC by MNSBC. The porous structure parameters listed in Table 1 demonstrated that
163 the S_{BET} and V_{tot} of biochars increased with pyrolysis temperature, and MSBC, NSBC and MNSBC
164 had the larger S_{BET} and V_{tot} ($S_{BET}=113-243$ m²/g and $V_{tot}=0.240-0.469$ cm³/g) than those of SBC
165 ($S_{BET}=44.1-76.5$ m²/g and $V_{tot}=0.115-0.227$ cm³/g). This result illustrated that FeCl₃ and CO(NH₂)₂
166 could react with carbon matrix of SBC and increase its porous structure [3].

167 The surface functional groups on the obtained biochar were presented in Fig. 1(b). The wide
168 bands located at 3408-3444 cm⁻¹ were identified as -OH. The characteristic bands at 1599-1622
169 cm⁻¹ and 1029-1039 cm⁻¹ corresponded to the presence of carboxylic C=O and C-O, respectively
170 [36,37]. The adsorption peaks of C-N (1397 cm⁻¹) and Fe-O (550 cm⁻¹) appeared on MNSBC
171 surface after FeCl₃ and CO(NH₂)₂ activation, which suggested that N and Fe had embedded into
172 the carbon structure [3]. The band position of Fe-O on MNSBC shifted after TC adsorption, which
173 indicated that it was capable of capturing TC by surface complexation [14]. The -OH on biochar
174 surface was regarded as the predominant functional group because it could bring H-bonding

175 interaction between it (H-donor) and nitrogen, oxygen atoms and aromatic rings of TC
176 (H-acceptors). The position and intensity of -OH on MNSBC changed after TC adsorption which
177 confirmed H-bonding was generated between TC and MNSBC [38]. The stretching vibration
178 intensity of -OH and C=O on MNSBC significantly decreased after TC adsorption, which was
179 assigned to the Lewis acid-base interaction between Lewis acids (-OH and C=O) on MNSBC and
180 Lewis base (-NH₂) on TC [39]. Additionally, the stretching vibration intensity of
181 oxygen-containing functional groups (-OH, C=O and C-O) on SBC decreased with increasing
182 pyrolysis temperature.

183 The Raman spectra of SBC and MNSBC were listed in Fig. 1(f). Two typical characteristic
184 peaks around 1344-1348 cm⁻¹ and 1585-1586 cm⁻¹ distributed on the Raman spectra of SBC and
185 MNSBC were defined as D-band and G-band, respectively [40]. The stretching vibration of
186 D-band was related to sp³ hybrid configuration of carbon atom, which reflected the carbon
187 framework defect of biochar. While, G-band described the sp² hybridization vibration of graphitic
188 structure. The value of I_D/I_G could be used to evaluate the graphitization degree of biochar [3]. The
189 I_D/I_G values of SBC and MNSBC were 1.45 and 1.25, respectively. Consistent with the above
190 XRD analysis, the lower I_D/I_G value of MNSBC also confirmed that FeCl₃ and CO(NH₂)₂
191 co-modification enhanced the graphitization degree of SBC, which facilitated the π - π conjugation
192 between MNSBC and TC.

193 The SEM-EDS images of SBC and MNSBC were listed in Fig. 2. The results showed that the
194 surface of SBC was smooth, and no obvious pore channels or sheets were observed on its surface
195 (Fig. 2(a)). While, MNSBC exhibited a rough surface with numerous porous and branch structure,
196 and this characteristic improved its porous structure which could provide abundant active sites for

197 TC adsorption (Fig. 2(b)). The results of elemental mapping showed that the main elemental
198 components of SBC and MNSBC were C, O and Si. While the content of Fe and N on MNSBC
199 increased, which suggested that Fe and N were successfully inserted into its carbon skeleton.

200 XPS spectra was used to investigate the elemental composition and chemical form of
201 biochars. The XPS survey spectra (Fig. 3(a)) showed that SBC and MNSBC had distinct C 1s
202 (284.8 eV) and O 1s (532.0 eV) peaks. The new peaks of N 1s at 400.5 eV and Fe 2p at 712.2 eV
203 in MNSBC spectra clearly illustrated successful embedding of N and Fe in its carbon matrix. The
204 C 1s of SBC, MNSBC and MNSBC-TC could be divided into three contributions of C-C/C=C
205 (284.8 eV), C-O (285.9, 286.0 and 286.4 eV) and C=O (289.0, 289.1 and 288.5 eV) (Fig. 3(b)).
206 Compared with SBC (C-C/C=C, 68.4%), the greater C-C/C=C content (70.4%) of MNSBC
207 described its greater graphitization degree [32]. This result was consistent with the above XRD
208 and Raman spectra analysis. Additionally, the C-C/C=C ratio of MNSBC reduced after TC
209 adsorption, suggesting its graphitic structure participated in π - π conjugation which facilitated TC
210 adsorption (Fig. 3(b)). The N 1s of MNSBC was decomposed into four related sub-peaks:
211 pyridinic-N (398.9 eV, 17.0%), pyrrolic-N (400.3 eV, 34.7%), graphitic-N (401.7 eV, 29.5%) and
212 oxidic-N (402.6 eV, 18.8%) [41] (Fig. 3(c)). Compared with MNSBC, the decrease in bonding
213 energy and content of pyridinic-N of MNSBC-TC was due to the Lewis acid-base interaction
214 between pyridinic-N of MNSBC (Lewis base) and -OH of TC (Lewis acid) [22]. In addition, the
215 content and bonding energy of pyrrolic-N on MNSBC surface also decreased. This was assigned
216 to the fact that the introduction of strongly electronegative N atoms reduced the electron density of
217 MNSBC surface [22,42], which enhanced the π - π conjugation interaction between MNSBC
218 (π -electron acceptor) and aromatic rings of TC (π -electron donor) and caused the reduction of

219 pyrrolic-N [43]. The Fe 2p of MNSBC could be decomposed into four peaks of Fe²⁺ 2p_{3/2} (711.9
220 eV), Fe³⁺ 2p_{3/2} (714.6 eV), Fe²⁺ 2p_{1/2} (725.2.9 eV) and Fe³⁺ 2p_{1/2} (728.0 eV) (Fig. 3(d)), which
221 further confirmed that magnetic Fe₃O₄ was successfully loaded on the surface of MNSBC due to
222 the co-existence of Fe²⁺ and Fe³⁺ [44]. The bonding energies of Fe²⁺ 2p_{3/2}, Fe³⁺ 2p_{3/2}, Fe²⁺ 2p_{1/2}
223 and Fe³⁺ 2p_{1/2} of MNSBC decreased after TC adsorption, indicating that complexation interaction
224 was involved between Fe₃O₄ and TC.

225 *3.2 The adsorption capacity of biochars and effect of MNSBC dose on TC removal*

226 Obviously, the adsorption capacity of SBC increased with pyrolysis temperature increasing
227 (Fig. 4(a)) because its greater graphitization degree and superior porous structure prepared at the
228 higher pyrolysis temperature. While no significant difference in the adsorption capacity of SBC
229 and SBC-973, which might be due to the significant decrease in the number of oxygen-containing
230 functional groups on SBC-973 surface. Fig. S1(a) described that the adsorption capacity of N-doped
231 SBC increased with the mass ratio of CO(NH₂)₂/SBC from 0.5:1 to 2:1. While no significant
232 difference in the adsorption capacity of NSBC-1 and NSBC-2 was observed, herein the mass ratio of
233 CO(NH₂)₂/SBC=1:1 was used to modify SBC. Fig. 4 (b) showed the increase in adsorption capacity
234 of SBC, MSBC, NSBC and MNSBC for TC with increasing reaction time. MNSBC exhibited a
235 greater adsorption capacity compared to SBC, MSBC and NSBC. The adsorption capacity of
236 MNSBC was 2.18, 1.66 and 1.06 times those of SBC, MSBC and NSBC, respectively. The effect
237 of MNSBC dose in the range of 15-35 mg on TC removal efficiencies was presented in Fig. S1(b).
238 Clearly, the removal efficiencies of TC increased with MNSBC dose because the higher dose could
239 provide more active sites for TC adsorption. The results showed that the removal rates were 70.2%,
240 80.4%, 92.3%, 94.2% and 95.3% for 15 mg, 10 mg, 25 mg, 30 mg and 35 mg of MNSBC, respectively.

241 Considering the economic cost and high removal efficiency, hence the dose of 25 mg MNSBC was
242 used in the subsequent experiments.

243 3.3 Adsorption kinetics of SBC and MNSBC

244 Fig. 4(c and d) showed that the adsorption capacity of biochars depended on the reaction time
245 at the specific TC concentration ($C_0=20$ mg/L). Unsurprisingly, the fastest adsorption occurred at
246 the initial stage, then the adsorption rate dropped dramatically and eventually achieved
247 equilibrium. The initial 240 min was identified as the rapid adsorption process, and about 80.0%
248 and 81.7% of the equilibrium adsorption amount of SBC and MNSBC for TC were accomplished
249 in this stage, respectively. This was due to the weaker diffusion resistance and large numbers of
250 unoccupied active sites. After this stage, the adsorption rate decreased as the concentration of TC
251 decreased and most of the binding sites had been occupied by TC molecules.

252 Pseudo-first/second-order, and Elovich models (their equations were listed in Text S3) were
253 applied to describe the experimental data of kinetics to study the adsorption mechanisms (Fig. 4
254 (c)). Pseudo-first-order model assumed that the adsorption rate of biochar was proportional to the
255 ratio of adsorbate concentration/biochar mass [36]. Pseudo-second-order model illustrated that the
256 adsorption process was mainly controlled by the chemical mechanisms including valency forces or
257 electrons exchange [45]. Elovich was another kinetics model used to describe the chemisorption of
258 solid-liquid [34]. The kinetics fitting parameters in Table S1 suggested that Elovich model better
259 describing the adsorption process of TC onto SBC and MNSBC with the greater non-linear
260 correlation coefficient ($R^2=0.989$ and 0.995) than those of pseudo-first-order ($R^2=0.926$ and 0.864)
261 and pseudo-second-order ($R^2=0.985$ and 0.968), also the equilibrium adsorption amount calculated
262 ($q_{e, cal}$ (mg/g)) from Elovich agreed better with the experimental value ($q_{e, exp}$ (mg/g)). The

263 parameters of a and b in Elovich model were related to the initial adsorption rate constant and
264 desorption rate constant, respectively. The greater ratio value of a/b suggested that the adsorption
265 process of TC onto MNSBC was favorable and irreversible [46], which indicated that a low risk of
266 the adsorbed TC being released into the solution again.

267 Intraparticle diffusion (its equation was listed in Text S3) was used to investigate the
268 diffusion mechanisms, as well as the dominant rate-limiting step [36]. The fitting plots of q_t
269 against $t^{1/2}$ were divided into two stages, and the first stage was named as liquid-film diffusion and
270 the second one was intraparticle diffusion (Fig. 4(d)). Two plots didn't pass through the origin
271 which suggested that intraparticle diffusion was not the unique rate-limiting step and the whole
272 adsorption process was simultaneously controlled by both liquid-film and intraparticle diffusions.
273 Firstly, TC transported from the bulk solution to the external surface of biochar in the stage of
274 liquid-film diffusion, then the adsorbed TC on the outer surface of biochar gradually spread into
275 the inner pores of biochar. The diffusion rate constants of liquid-film diffusion ($K_f=1.61$ mg/g
276 min^{1/2} and 3.14 mg/g min^{1/2}) were greater than those of intraparticle diffusion ($K_{II}=0.288$ mg/g
277 min^{1/2} and 0.435 mg/g min^{1/2}) despite of biochars (Table S2), which illustrated that the step of
278 liquid-film diffusion was more distinct. In addition, the liquid-film diffusion and intraparticle
279 diffusion constants ($K_f=3.14$ mg/g min^{1/2} and $K_{II}=0.435$ mg/g min^{1/2}) of MNSBC were greater than
280 those of SBC ($K_f=1.61$ mg/g min^{1/2} and $K_{II}=0.288$ mg/g min^{1/2}) which might be due to its larger
281 S_{BET} and V_{tot} confirmed in BET analysis. More than 80% of the adsorption capacity was
282 accomplished in the stage of liquid-film diffusion, which suggested that the contribution of TC
283 adsorption through liquid-film diffusion was larger than that of intraparticle diffusion. C was
284 related to the thickness of boundary layer, and C_{II} values were higher than the values of C_I , which

285 demonstrated that the resistance of intraparticle diffusion was greater than that of liquid-film
286 diffusion. This phenomenon was mainly attributed to the larger numbers of unoccupied active sites
287 in the stage of liquid-film diffusion, while most of these active sites had been occupied by TC in
288 the stage of intraparticle diffusion [46].

289 3.4 Adsorption isotherms

290 As shown in Fig. 5(a), the equilibrium adsorption amounts of TC on SBC and MNSBC and
291 concentrations of TC increased with the initial concentrations of TC (from 20 mg/L to 200 mg/L).
292 Adsorption isotherms described TC was in dynamic equilibrium between solid and liquid at
293 various concentrations. Four isotherm models including Langmuir, Freundlich, Temkin and
294 Dubinin–Radushkevich (their equations were listed in Text S3) were adopted to fit the
295 experimental data in this study. Langmuir model was proposed based on the hypothesis that the
296 adsorption process was mainly a monolayer chemisorption, and biochar surface was homogeneous.
297 While, Freundlich model assumed that it was a multi-layer physisorption, bonding energy was not
298 equal and the biochar surface was heterogeneous [47]. Generally, Langmuir isotherms model
299 could be applied to estimate the maximal adsorption amounts of biochar. The maximal TC
300 adsorption amounts of MNSBC and SBC calculated by this model were 197.3 mg/g and 63.3 mg/g,
301 respectively. The adsorption capacity of MNSBC (197.3 mg/g) prepared here was significantly
302 larger than those of SBC (63.3 mg/g) (this study), magnetic *Auricularia Auricula* dregs biochar
303 (42.31 mg/g) [48], alkali modified magnetic rice straw biochar (97.86 mg/g) [14] and spent coffee
304 ground derived biochar (39.22 mg/g) [49]. The fitting results (Fig. 5(a)) and parameters (Table S3)
305 suggested that the isotherms data of SBC and MNSBC agreed better with Freundlich model with
306 the greater non-linear correlation coefficient ($R^2=0.998$ and 0.993), also $0 < 1/n < 1$ suggested that

307 this isotherm model was favorable. This result indicated that the adsorption processes of TC onto
308 SBC/MNSBC were multi-layer physisorption on their homogeneous surfaces [50]. To further
309 verify the adsorption process of TC onto biochar, Temkin and Dubinin–Radushkevich models
310 were also adopted to fit the experimental data of isotherms. Temkin model described that the
311 adsorption energy was uniformly distributed and it decreased linearly with the surface coverage
312 [51]. It was more suitable for illustrating the chemical adsorption process, and its weaker
313 non-linear correlation coefficients ($R^2=0.982$ and 0.984) than those of Freundlich model suggested
314 that chemical interactions were not the only adsorption mechanism. The free energy (E
315 $(\text{kJ/mol})=1/\sqrt{2\beta}$) calculated from Dubinin–Radushkevich model could be used to distinguish the
316 adsorption interactions of physical or chemical [52]. The E values lied between 20 kJ/mol and 40
317 kJ/mol, which described the chemical interactions were also involved in the adsorption processes
318 of TC adsorption onto SBC and MNSBC.

319 *3.5 Adsorption thermodynamics*

320 Adsorption thermodynamic experiments were conducted to identify the effect of reaction
321 temperature on the adsorption performance of MNSBC for TC. Fig. 5(b) showed that the
322 equilibrium adsorption amounts of MNSBC increased with the initial TC concentration and
323 reaction temperature. This result suggested that the process of TC adsorption onto MNSBC was
324 endothermic. All the parameters calculated by the Gibbs-Helmholtz equations were listed in Table
325 S4. The parameter of $\Delta H > 0$ further confirmed it was an endothermic adsorption process [53]. All
326 the values of ΔG were negative, which illustrated that TC adsorption onto MNSBC was favorable
327 and spontaneous [38]. And, the absolute ΔG value increased with the reaction temperature, which
328 suggested that increasing reaction temperature enhanced the spontaneity of TC adsorption onto

329 MNSBC. In addition, the positive ΔS value demonstrated that the randomness increased on the
330 solid-liquid interface during the process of TC adsorption onto MNSBC.

331 *3.6 Effect of environmental factors*

332 Previous studies described that environmental factor had a significant effect on the adsorption
333 performance of biochar [54,55]. Representative indexes, such as solution pH, ionic
334 species/strength and HA concentration were conducted here to study their effect on TC removal by
335 MNSBC. The electrostatic attraction/repulsion were mainly determined by the ionization species
336 of TC and surface charge of MNSBC. TC was an amphoteric molecule due to its acidic group
337 (phenolic -OH) and basic group (-NH₂). Solution pH was considered as a critical environmental
338 factor controlling the whole adsorption process because it could simultaneously determine the
339 form of TC and zeta potential of MNSBC. Three dissociation constants of TC ($pK_{a1}=3.3$, $pK_{a2}=7.7$
340 and $pK_{a3}=9.7$) decided its four kinds of existing form at different solution pH. Generally, TC was
341 in form of TC⁺ at pH<3.3, TC⁰ at 3.3<pH<7.7, TC⁻ at 7.7<pH<9.7, and TC²⁻ at pH>9.7 (the species
342 distribution calculation of TC was summarized in Text S4) (Fig. 6(a)). Fig. 6(d) described that the
343 zeta potential of MNSBC decreased with pH increasing and the point of zero potential charge
344 (pH_{ZPC}) of MNSBC was 3.45. It was well accepted that the biochar surface was positively charged
345 when the solution pH was below its pH_{ZPC} and bond to the anions, otherwise its surface was
346 negatively charged and bond to the cations. Obviously, MNSBC showed the optimum adsorption
347 performance for TC at pH=5 because TC was in the form of TC⁰, and no electrostatic repulsion
348 was existed between MNSBC and TC. The adsorption capacity of MNSBC was inhibited above or
349 below this pH due to the electrostatic repulsion formation between TC and MNSBC as they were
350 simultaneously positively or negatively charged. Additionally, TC could act as the Lewis acid

351 because of its phenolic -OH, and TC began to deprotonate around pH=8, and this phenomenon
352 became more apparent when pH>9.7. OH⁻ as the Lewis base could easily attract the proton of the
353 phenolic -OH, resulting in the deprotonation of TC and breaking the hydrogen bond between TC
354 and MNSBC [54,55]. Above pH=9, the intensity of electrostatic repulsion significantly increased
355 because the surface of MNSBC was more negatively charged and TC was mainly in the form of
356 TC²⁻, and the hydrophobicity of TC significantly reduced, while MNSBC still had considerable
357 adsorption performance for TC because charge assisted hydrogen bond (CAHB) became the main
358 adsorption force and participated in overcoming the increased electrostatic repulsion [56].

359 To study the effect of ionic species/strength on TC removal by MNSBC, the adsorption
360 capacity of MNSBC was determined in the presence of NaCl, NaNO₃, NaH₂PO₄, NaHCO₃ and
361 CaCl₂. Fig. 6 (f-j) described that the adsorption capacity of MNSBC decreased with the ionic
362 strength increasing despite of the ionic species because these charged ionic compounds could
363 eliminate the repulsive interaction among adsorbents and facilitated them to generate more
364 compact aggregation structure (i.e. squeezing-out effect), which was unfavorable for TC
365 adsorption [55]. However, three inorganic salts of NaCl, NaNO₃ and NaH₂PO₄ showed no obvious
366 influence on TC removal by MNSBC, which might be due to the weak squeezing-out effect. To
367 identify the effect of HCO₃⁻ and H₂PO₄⁻, the solution pH was adjusted to 9 and 5 (the species
368 distribution calculation of H₂CO₃ and H₃PO₄ were given in Text S4), respectively (Fig. 6 (b and
369 c)). Apparently, the adsorption performance of MNSBC for TC was significantly inhibited in the
370 presence of NaHCO₃. This phenomenon was because the hydrolysis of HCO₃⁻ would cause the
371 alkaline environment and increase the electrostatic repulsion between TC and MNSBC. Also, the
372 existence of CaCl₂ significantly inhibited TC removal because Ca²⁺ could bind with the carboxyl

373 on MNSBC surface which disturbed the π - π conjugation between TC and MNSBC [1,57].
374 Additionally, Ca^{2+} could also bind with TC to form Ca-TC complex, which decreased the affinity
375 of MNSBC for TC [57]. HA was the common organic compound that widely distributed in natural
376 waters [58]. Particularly, the adsorption capacity of MNSBC decreased with the HA concentration
377 increasing because competitive adsorption occurred between TC and HA or generation of HA-TC
378 compound reduced the affinity of MNSBC for TC (Fig. 6(k)).

379 *3.7 Adsorption mechanisms*

380 The mechanisms of TC adsorption onto MNSBC were investigated by characterization,
381 adsorption model fitting and environmental factors experiments analysis. Elovich and Freundlich
382 models better fitted the kinetics and isotherms data, respectively, suggesting that the adsorption
383 process was simultaneously dominated by physicochemical interactions. The well developed
384 graphitic structure of MNSBC could interact with four aromatic rings in the molecular structure of
385 TC through π - π conjugation (XRD, Raman spectra and XPS analysis). Also, TC could react with
386 MNSBC through cation- π bond between the protonated amino groups and graphite π -electron
387 because its great ionization constant ($\text{p}K_{a3}$ value was 9.7) [59]. The C=O, -OH on MNSBC were
388 regarded as the Lewis acids and $-\text{NH}_2$ of TC acted as the Lewis base, which caused Lewis
389 acid-base interactions between MNSBC and TC. Additionally, the presence of pyridinic-N on
390 MNSBC (Lewis base) could enhance the Lewis acid-base interaction between MNSBC and
391 phenolic -OH of TC (Lewis acid). The reduction of pyrrolic N on MNSBC after TC adsorption
392 suggested that the introduction of strongly electronegative N atoms reduced the electron density of
393 MNSBC surface, which enhanced the π - π conjugation interaction between MNSBC (π -electron
394 acceptor) and aromatic rings of TC (π -electron donor) (XPS analysis). The adsorption capacity of

395 MNSBC was significantly affected by solution pH and NaHCO₃ concentration, indicating that
396 electrostatic interaction could dominate the adsorption process. The inhibitory effect of CaCl₂ was
397 mainly attributed to Ca²⁺ which could destroy the π - π conjugation between TC and MNSBC by
398 binding with the carboxyl on MNSBC surface. Also, Ca²⁺ could bind with TC to form Ca-TC
399 complex, which decreased the affinity of MNSBC for TC. The adsorption capacity of MNSBC
400 decreased in the presence of HA, which might be due to the competitive effect of HA or the
401 generation of HA-TC compound reducing the affinity of MNSBC for TC. MNSBC performed the
402 superior porous structure (larger S_{BET} and V_{tot}) than that of SBC, which provided abundant binding
403 sites for TC adsorption by pore filling (SEM and BET analysis). The decrease in bonding energy
404 of Fe 2p (Fe²⁺ 2p_{3/2}, Fe³⁺ 2p_{3/2}, Fe²⁺ 2p_{1/2} and Fe³⁺ 2p_{1/2}) (XPS analysis) and change of Fe-O band
405 (FTIR analysis) on MNSBC after TC adsorption illustrated that Fe₃O₄ could adsorb TC through
406 surface complexation. The thermodynamic parameters suggested that the process of TC adsorption
407 onto MNSBC was spontaneous, endothermic and randomness increasing.

408 *3.8 The adsorption performance of MNSBC for TC in various real waters*

409 Various real water samples, including deionized, mineral, tap, lake and river waters (the basic
410 physicochemical properties of these waters were listed in Table S5) were conducted in this study
411 to further verify the adsorption performance of MNSBC for TC. The water samples of tap water
412 and mineral water were obtained from Wuhan University of Technology and Wuhan Mingxinquan
413 Pure Water Co., Ltd., respectively. Lake water and river water were collected at south lake of
414 Wuhan (30°50' N, 114°35' E) and Wuhan section of Yangtze River (30°10' N, 114°09' E),
415 respectively. Considering that the real environmental waters might affect the results measured by
416 ultraviolet spectrophotometry, the residual concentrations of TC in these real waters were

417 determined by high performance liquid chromatography (HPLC, 1260 Infinity, Agilent
418 Technologies) equipped with a ZORBAX SB-C18 column (5 μm , 4.6 \times 150 mm, Agilent) at the
419 determination wavelength of 360 nm. The mobile phase was a mixture of 0.1% formic acid and
420 methanol (V/V=75/25) with a flow rate of 0.8 mL/min. Fig. 7(a) showed that MNSBC had
421 excellent TC adsorption performance in deionized water (93.4%), mineral water (91.6%), tap
422 water (89.0%), lake water (82.1%), and river water (80.8%). The removal efficiency of TC in lake
423 water and river water by MNSBC were slightly inhibited, which might be related to the inorganic
424 compounds (e.g., N and P) had occupied some active sites of MNSBC because the concentrations
425 of TN (reduced by 73.6% and 66.7%, respectively) and TP (reduced by 71.7% and 71.1%,
426 respectively) were significantly decreased after adsorption.

427 *3.9 The regeneration and environmental safety of MNSBC*

428 The possibility to regenerate biochar after TC adsorption is a critical indicator to determine
429 economic feasibility of its use [60]. Two inorganic solvents, namely HCl (0.1 mol/L) and NaOH
430 (0.1 mol/L) were used to regenerate MNSBC in this study because the solubility of TC would
431 increase in the acidic or alkaline condition which facilitated the adsorbed TC to release into the
432 solution, and H₂O treatment as control. Also, the protonation state of the surface functional groups
433 would change when using acid or alkali to regenerate adsorbent, breaking the adsorption
434 equilibrium resulting in the desorption of the adsorbate from the adsorbent [1]. The results
435 presented in Fig. 7(b) demonstrated that the adsorption capacity of the used MNSBC decreased
436 using H₂O and HCl regeneration in the reuse cycles. After five reuse cycles, the adsorption
437 capacity of MNSBC were 15.3% and 40.3% of its initial performance by H₂O and HCl treatment,
438 respectively. While, MNSBC maintained a high TC adsorption capacity (97.9% of the initial

439 adsorption capacity) even after five cycles of reuse using NaOH regeneration, which suggested
440 that MNSBC was a promising adsorbent with excellent sustainable adsorption performance by
441 NaOH regeneration.

442 As leaching of N into water bodies could result in eutrophication, and release of Fe might
443 cause secondary water pollution, the extent to which N and Fe was released by the MNSBC in
444 different pH environments was assessed. Results in Fig. 7(c and d) showed that the leaching levels
445 of Fe and TN were below the national (China) environmental limit values of GB 3838-2002
446 ($C(\text{Fe})=0.3$ mg/L and $C(\text{TN})=0.2$ mg/L (I category water)) at all pH levels tested in this study.
447 This result suggested that MNSBC could be applied safely in water treatment, at least from the
448 perspective of Fe and N release.

449 **4. Conclusions**

450 This study successfully synthesized the MNSBC, which showed excellent adsorption
451 capacity for TC as a result of its superior physicochemical characteristics (e.g., larger S_{BET} , V_{tot} ,
452 greater graphitization degree and N-doping). Lewis acid-base, π - π conjugation, electrostatic
453 interactions and pore filling were identified as the main adsorption mechanisms. The added N and
454 Fe were safely embedded in the carbon matrix of the MNSBC, as demonstrated by leaching tests
455 at different pH levels (from 3 to 11). Furthermore, MNSBC showed a sustained adsorption
456 capacity even after multiple cycles of regeneration using NaOH, maintaining over 97% of its
457 capacity after five cycles. The excellent TC adsorption performance of MNSBC was demonstrated
458 not only in simulated water samples using deionized water, but also real water samples using
459 mineral water, tap water, lake water and river water, indicating a true potential for real world
460 application. This study identified a promising approach for municipal sludge resource utilization

461 in water treatment for removal of TC, and potentially other applications.

462 **Acknowledgements**

463 This work was supported by the National Natural Science Foundation of China (No. 52170171,

464 and No.51878523), Central Public-interest Scientific Institution Basal Research Fund (No.

465 Y2022GH10), the “111” Project of China and the Scottish Government’s Rural and Environment

466 Science and Analytical Service Division (RESAS).

467 **References**

- 468 [1] L. Yan, Y. Liu, Y. Zhang, S. Liu, C. Wang, W. Chen, C. Liu, Z. Chen, Y. Zhang, ZnCl₂ modified biochar
469 derived from aerobic granular sludge for developed microporosity and enhanced adsorption to tetracycline,
470 *Bioresour. Technol.* 297 (2020) 122381.
- 471 [2] Q. Zhang, G. Ying, C. Pan, Y. Liu, J. Zhao, Comprehensive Evaluation of Antibiotics Emission and Fate in
472 the River Basins of China: Source Analysis, Multimedia Modeling, and Linkage to Bacterial Resistance,
473 *Environ. Sci. Technol.* 49 (2015) 6772-6782.
- 474 [3] Y. Mei, J. Xu, Y. Zhang, B. Li, S. Fan, H. Xu, Effect of Fe–N modification on the properties of biochars and
475 their adsorption behavior on tetracycline removal from aqueous solution, *Bioresour. Technol.* 325 (2021)
476 124732.
- 477 [4] R. Daghrir, P. Drogui, Tetracycline antibiotics in the environment: a review, *Environ. Chem. Lett.* 11 (2013)
478 209-227.
- 479 [5] G. Chen, S. He, G. Shi, Y. Ma, C. Ruan, X. Jin, Q. Chen, X. Liu, H. Dai, X. Chen, D. Huang, In-situ
480 immobilization of ZIF-67 on wood aerogel for effective removal of tetracycline from water, *Chem. Eng. J.*
481 423 (2021) 130184.
- 482 [6] G. Wu, J. Ma, S. Li, J. Guan, B. Jiang, L. Wang, J. Li, X. Wang, L. Chen, Magnetic copper-based metal
483 organic framework as an effective and recyclable adsorbent for removal of two fluoroquinolone antibiotics
484 from aqueous solutions, *J. Colloid Interf. Sci.* 528 (2018) 360-371.
- 485 [7] X. Li, W. Zhu, G. Meng, C. Zhang, R. Guo, Efficiency and kinetics of conventional pollutants and
486 tetracyclines removal in integrated vertical-flow constructed wetlands enhanced by aeration, *J. Environ.*
487 *Manage.* 273 (2020) 111120.
- 488 [8] Q. Zhong, Q. Lin, W. He, H. Fu, Z. Huang, Y. Wang, L. Wu, Study on the nonradical pathways of

489 nitrogen-doped biochar activating persulfate for tetracycline degradation, *Sep. Purif. Technol.* 276 (2021)
490 119354.

491 [9] L. Leng, L. Wei, Q. Xiong, S. Xu, W. Li, S. Lv, Q. Lu, L. Wan, Z. Wen, W. Zhou, Use of microalgae based
492 technology for the removal of antibiotics from wastewater: A review, *Chemosphere* 238 (2020) 124680.

493 [10] H.M. Jang, E. Kan, Engineered biochar from agricultural waste for removal of tetracycline in water, *Bioresour.*
494 *Technol.* 284 (2019) 437-447.

495 [11] L. Yi, L. Zuo, C. Wei, H. Fu, X. Qu, S. Zheng, Z. Xu, Y. Guo, H. Li, D. Zhu, Enhanced adsorption of
496 bisphenol A, tylosin, and tetracycline from aqueous solution to nitrogen-doped multiwall carbon nanotubes
497 via cation- π and π - π electron-donor-acceptor (EDA) interactions, *Sci. Total Environ.* 719 (2020) 137389.

498 [12] Z.A. AlOthman, N. AlMasoud, X.Y. Mbianda, I. Ali, Synthesis and characterization of
499 γ -cyclodextrin-graphene oxide nanocomposite: Sorption, kinetics, thermodynamics and simulation studies of
500 tetracycline and chlortetracycline antibiotics removal in water, *J. Mol. Liq.* (2021) 116993.

501 [13] M. Wu, S. Zhao, R. Jing, Y. Shao, X. Liu, F. Lv, X. Hu, Q. Zhang, Z. Meng, A. Liu, Competitive adsorption
502 of antibiotic tetracycline and ciprofloxacin on montmorillonite, *Appl. Clay Sci.* 180 (2019) 105175.

503 [14] J. Dai, X. Meng, Y. Zhang, Y. Huang, Effects of modification and magnetization of rice straw derived biochar
504 on adsorption of tetracycline from water, *Bioresour. Technol.* 311 (2020) 123455.

505 [15] X. Zhang, Y. Li, M. Wu, Y. Pang, Z. Hao, M. Hu, R. Qiu, Z. Chen, Enhanced adsorption of tetracycline by an
506 iron and manganese oxides loaded biochar: Kinetics, mechanism and column adsorption, *Bioresour. Technol.*
507 320 (2021) 124264.

508 [16] G. Kor-Bicakci, C. Eskicioglu, Recent developments on thermal municipal sludge pretreatment technologies
509 for enhanced anaerobic digestion, *Renew. Sust. Energ. Rev.* 110 (2019) 423-443.

510 [17] A. Gopinath, G. Divyapriya, V. Srivastava, A.R. Laiju, P.V. Nidheesh, M.S. Kumar, Conversion of sewage

511 sludge into biochar: A potential resource in water and wastewater treatment, *Environ. Res.* 194 (2021)
512 110656.

513 [18] H. Liu, G. Xu, G. Li, Preparation of porous biochar based on pharmaceutical sludge activated by NaOH and
514 its application in the adsorption of tetracycline, *J. Colloid Interf. Sci.* 587 (2021) 271-278.

515 [19] Y. Ma, P. Li, L. Yang, L. Wu, L. He, F. Gao, X. Qi, Z. Zhang, Iron/zinc and phosphoric acid modified sludge
516 biochar as an efficient adsorbent for fluoroquinolones antibiotics removal, *Ecotox. Environ. Safe.* 196 (2020)
517 110550.

518 [20] O. Paunovic, S. Pap, S. Maletic, M.A. Taggart, N. Boskovic, M. Turk Sekulic, Ionisable emerging
519 pharmaceutical adsorption onto microwave functionalised biochar derived from novel lignocellulosic waste
520 biomass, *J. Colloid Interf. Sci.* 547 (2019) 350-360.

521 [21] Y. Wu, H. Cheng, D. Pan, L. Zhang, W. Li, Y. Song, Y. Bian, X. Jiang, J. Han, Potassium
522 hydroxide-modified algae-based biochar for the removal of sulfamethoxazole: Sorption performance and
523 mechanisms, *J. Environ. Manage.* 293 (2021) 112912.

524 [22] L. Wang, W. Yan, C. He, H. Wen, Z. Cai, Z. Wang, Z. Chen, W. Liu, Microwave-assisted preparation of
525 nitrogen-doped biochars by ammonium acetate activation for adsorption of acid red 18, *Appl. Surf. Sci.* 433
526 (2018) 222-231.

527 [23] Y. Ma, L. Yang, L. Wu, P. Li, X. Qi, L. He, S. Cui, Y. Ding, Z. Zhang, Carbon nanotube supported sludge
528 biochar as an efficient adsorbent for low concentrations of sulfamethoxazole removal, *Sci. Total Environ.*
529 718 (2020) 137299.

530 [24] L. Leng, S. Xu, R. Liu, T. Yu, X. Zhuo, S. Leng, Q. Xiong, H. Huang, Nitrogen containing functional groups
531 of biochar: An overview, *Bioresour. Technol.* 298 (2020) 122286.

532 [25] X. Pei, X. Peng, X. Jia, P.K. Wong, N-doped biochar from sewage sludge for catalytic peroxydisulfate

533 activation toward sulfadiazine: Efficiency, mechanism, and stability, *J. Hazard. Mater.* 419 (2021) 126446.

534 [26] T. Nguyen, Q. Truong, C. Chen, R. Doong, W. Chen, C. Dong, Mesoporous and adsorption behavior of algal

535 biochar prepared via sequential hydrothermal carbonization and ZnCl₂ activation, *Bioresour. Technol.* (2021)

536 126351.

537 [27] Y. Ma, M. Li, P. Li, L. Yang, L. Wu, F. Gao, X. Qi, Z. Zhang, Hydrothermal synthesis of magnetic sludge

538 biochar for tetracycline and ciprofloxacin adsorptive removal, *Bioresour. Technol.* 319 (2021) 124199.

539 [28] Y. Ma, T. Lu, L. Yang, L. Wu, P. Li, J. Tang, Y. Chen, F. Gao, S. Cui, X. Qi, Z. Zhang, Efficient adsorptive

540 removal of fluoroquinolone antibiotics from water by alkali and bimetallic salts co-hydrothermally modified

541 sludge biochar, *Environ. Pollut.* 298 (2022) 118833.

542 [29] W. Cai, J. Wei, Z. Li, Y. Liu, J. Zhou, B. Han, Preparation of amino-functionalized magnetic biochar with

543 excellent adsorption performance for Cr(VI) by a mild one-step hydrothermal method from peanut hull,

544 *Colloids Surf. A.* (2019) 102-111.

545 [30] W. Zhao, Y. Tian, X. Chu, L. Cui, H. Zhang, M. Li, P. Zhao, Preparation and characteristics of a magnetic

546 carbon nanotube adsorbent: Its efficient adsorption and recoverable performances, *Sep. Purif. Technol.* 257

547 (2021) 117917.

548 [31] J. Wei, Y. Liu, J. Li, Y. Zhu, H. Yu, Y. Peng, Adsorption and co-adsorption of tetracycline and doxycycline

549 by one-step synthesized iron loaded sludge biochar, *Chemosphere* 236 (2019) 124254.

550 [32] S. Ho, Y. Chen, R. Li, C. Zhang, Y. Ge, G. Cao, M. Ma, X. Duan, S. Wang, N. Ren, N-doped graphitic

551 biochars from C-phycoyanin extracted *Spirulina* residue for catalytic persulfate activation toward nonradical

552 disinfection and organic oxidation, *Water Res.* 159 (2019) 77-86.

553 [33] W. Lu, J. Li, Y. Sheng, X. Zhang, J. You, L. Chen, One-pot synthesis of magnetic iron oxide

554 nanoparticle-multiwalled carbon nanotube composites for enhanced removal of Cr(VI) from aqueous

555 solution, *J. Colloid Interf. Sci.* 505 (2017) 1134-1146.

556 [34] S. Álvarez-Torrellas, M. Muñoz, J.A. Zazo, J.A. Casas, J. García, Synthesis of high surface area carbon
557 adsorbents prepared from pine sawdust- *Onopordum acanthium* L. for nonsteroidal anti-inflammatory drugs
558 adsorption, *J. Environ. Manage.* 183 (2016) 294-305.

559 [35] L. Tang, J. Yu, Y. Pang, G. Zeng, Y. Deng, J. Wang, X. Ren, S. Ye, B. Peng, H. Feng, Sustainable efficient
560 adsorbent: Alkali-acid modified magnetic biochar derived from sewage sludge for aqueous organic
561 contaminant removal, *Chem. Eng. J.* 336 (2018) 160-169.

562 [36] X. Geng, S. Lv, J. Yang, S. Cui, Z. Zhao, Carboxyl-functionalized biochar derived from walnut shells with
563 enhanced aqueous adsorption of sulfonamide antibiotics, *J. Environ. Manage.* 280 (2021) 111749.

564 [37] X. Feng, B. Qiu, D. Sun, Enhanced naproxen adsorption by a novel β -cyclodextrin immobilized the
565 three-dimensional macrostructure of reduced graphene oxide and multiwall carbon nanotubes, *Sep. Purif.*
566 *Technol.* 290 (2022) 120837.

567 [38] T. Atugoda, C. Gunawardane, M. Ahmad, M. Vithanage, Mechanistic interaction of ciprofloxacin on zeolite
568 modified seaweed (*Sargassum crassifolium*) derived biochar: Kinetics, isotherm and thermodynamics,
569 *Chemosphere* 281 (2021) 130676.

570 [39] H. Zhao, X. Liu, Z. Cao, Y. Zhan, X. Shi, Y. Yang, J. Zhou, J. Xu, Adsorption behavior and mechanism of
571 chloramphenicols, sulfonamides, and non-antibiotic pharmaceuticals on multi-walled carbon nanotubes, *J.*
572 *Hazard. Mater.* 310 (2016) 235-245.

573 [40] W. Shi, H. Wang, J. Yan, L. Shan, G. Quan, X. Pan, L. Cui, Wheat straw derived biochar with hierarchically
574 porous structure for bisphenol A removal: Preparation, characterization, and adsorption properties, *Sep. Purif.*
575 *Technol.* 289 (2022) 120796.

576 [41] K. Zhong, M. Li, Y. Yang, H. Zhang, B. Zhang, J. Tang, J. Yan, M. Su, Z. Yang, Nitrogen-doped biochar

577 derived from watermelon rind as oxygen reduction catalyst in air cathode microbial fuel cells, *Appl. Energ.*
578 242 (2019) 516-525.

579 [42] L. Wang, D. Zhu, L. Duan, W. Chen, Adsorption of single-ringed N- and S-heterocyclic aromatics on carbon
580 nanotubes, *Carbon* 48 (2010) 3906-3915.

581 [43] F. Lian, G. Cui, Z. Liu, L. Duo, G. Zhang, B. Xing, One-step synthesis of a novel N-doped microporous
582 biochar derived from crop straws with high dye adsorption capacity, *J. Environ. Manage.* 176 (2016) 61-68.

583 [44] M. Jia, Z. Yang, W. Xiong, J. Cao, Y. Xiang, H. Peng, Y. Jing, C. Zhang, H. Xu, P. Song, Magnetic
584 heterojunction of oxygen-deficient Ti³⁺-TiO₂ and Ar-Fe₂O₃ derived from metal-organic frameworks for
585 efficient peroxydisulfate (PDS) photo-activation, *Appl. Catal. B.* 298 (2021) 120513.

586 [45] X. Liu, Y. Guo, C. Zhang, X. Huang, K. Ma, Y. Zhang, Preparation of graphene oxide/4A molecular sieve
587 composite and evaluation of adsorption performance for Rhodamine B, *Sep. Purif. Technol.* 286 (2022)
588 120400.

589 [46] K.C. Bedin, A.C. Martins, A.L. Cazetta, O. Pezoti, V.C. Almeida, KOH-activated carbon prepared from
590 sucrose spherical carbon: Adsorption equilibrium, kinetic and thermodynamic studies for Methylene Blue
591 removal, *Chem. Eng. J.* 286 (2016) 476-484.

592 [47] C. Hu, J. Jiang, Y. Li, Y. Wu, J. Ma, H. Li, H. Zheng, Eco-friendly poly(dopamine)-modified glass
593 microspheres as a novel self-floating adsorbent for enhanced adsorption of tetracycline, *Sep. Purif. Technol.*
594 292 (2022) 121046.

595 [48] F. Gao, Z. Xu, Y. Dai, Removal of tetracycline from wastewater using magnetic biochar: A comparative study
596 of performance based on the preparation method, *Environ. Technol. Inno.* 24 (2021) 101916.

597 [49] V. Nguyen, T. Nguyen, C. Chen, C. Hung, T. Vo, J. Chang, C. Dong, Influence of pyrolysis temperature on
598 polycyclic aromatic hydrocarbons production and tetracycline adsorption behavior of biochar derived from

599 spent coffee ground, *Bioresour. Technol.* 284 (2019) 197-203.

600 [50] A.R. Bagheri, M. Arabi, M. Ghaedi, A. Ostovan, X. Wang, J. Li, L. Chen, Dummy molecularly imprinted
601 polymers based on a green synthesis strategy for magnetic solid-phase extraction of acrylamide in food
602 samples, *Talanta* 195 (2019) 390-400.

603 [51] Y. Sun, H. Li, G. Li, B. Gao, Q. Yue, X. Li, Characterization and ciprofloxacin adsorption properties of
604 activated carbons prepared from biomass wastes by H₃PO₄ activation, *Bioresour. Technol.* 217 (2016)
605 239-244.

606 [52] Y. Zhou, X. Liu, Y. Xiang, P. Wang, J. Zhang, F. Zhang, J. Wei, L. Luo, M. Lei, L. Tang, Modification of
607 biochar derived from sawdust and its application in removal of tetracycline and copper from aqueous
608 solution: Adsorption mechanism and modelling, *Bioresour. Technol.* 245 (2017) 266-273.

609 [53] W. Deng, D. Zhang, X. Zheng, X. Ye, X. Niu, Z. Lin, M. Fu, S. Zhou, Adsorption recovery of phosphate from
610 waste streams by Ca/Mg-biochar synthesis from marble waste, calcium-rich sepiolite and bagasse, *J. Clean.*
611 *Prod.* 288 (2021) 125638.

612 [54] Q. Duan, X. Li, Z. Wu, A. Alsaedi, T. Hayat, C. Chen, J. Li, Adsorption of 17 β -estradiol from aqueous
613 solutions by a novel hierarchically nitrogen-doped porous carbon, *J. Colloid Interf. Sci.* 533 (2019) 700-708.

614 [55] L. Jiang, Y. Liu, S. Liu, X. Hu, G. Zeng, X. Hu, S. Liu, S. Liu, B. Huang, M. Li, Fabrication of
615 β -cyclodextrin/poly (L -glutamic acid) supported magnetic graphene oxide and its adsorption behavior for
616 17 β -estradiol, *Chem. Eng. J.* 308 (2017) 597-605.

617 [56] C. Ling, X. Li, Z. Zhang, F. Liu, Y. Deng, X. Zhang, A. Li, L. He, B. Xing, High Adsorption of
618 Sulfamethoxazole by an Amine-Modified Polystyrene–Divinylbenzene Resin and Its Mechanistic Insight,
619 *Environ. Sci. Technol.* 50 (2016) 10015-10023.

620 [57] Y. Feng, G. Chen, Y. Zhang, D. Li, C. Ling, Q. Wang, G. Liu, Superhigh co-adsorption of tetracycline and

621 copper by the ultrathin g-C₃N₄ modified graphene oxide hydrogels, *J. Hazard. Mater.* 424 (2022) 127362.

622 [58] J. Han, W. Qiu, Z. Cao, J. Hu, W. Gao, Adsorption of ethinylestradiol (EE2) on polyamide 612: Molecular
623 modeling and effects of water chemistry, *Water Res.* 47 (2013) 2273-2284.

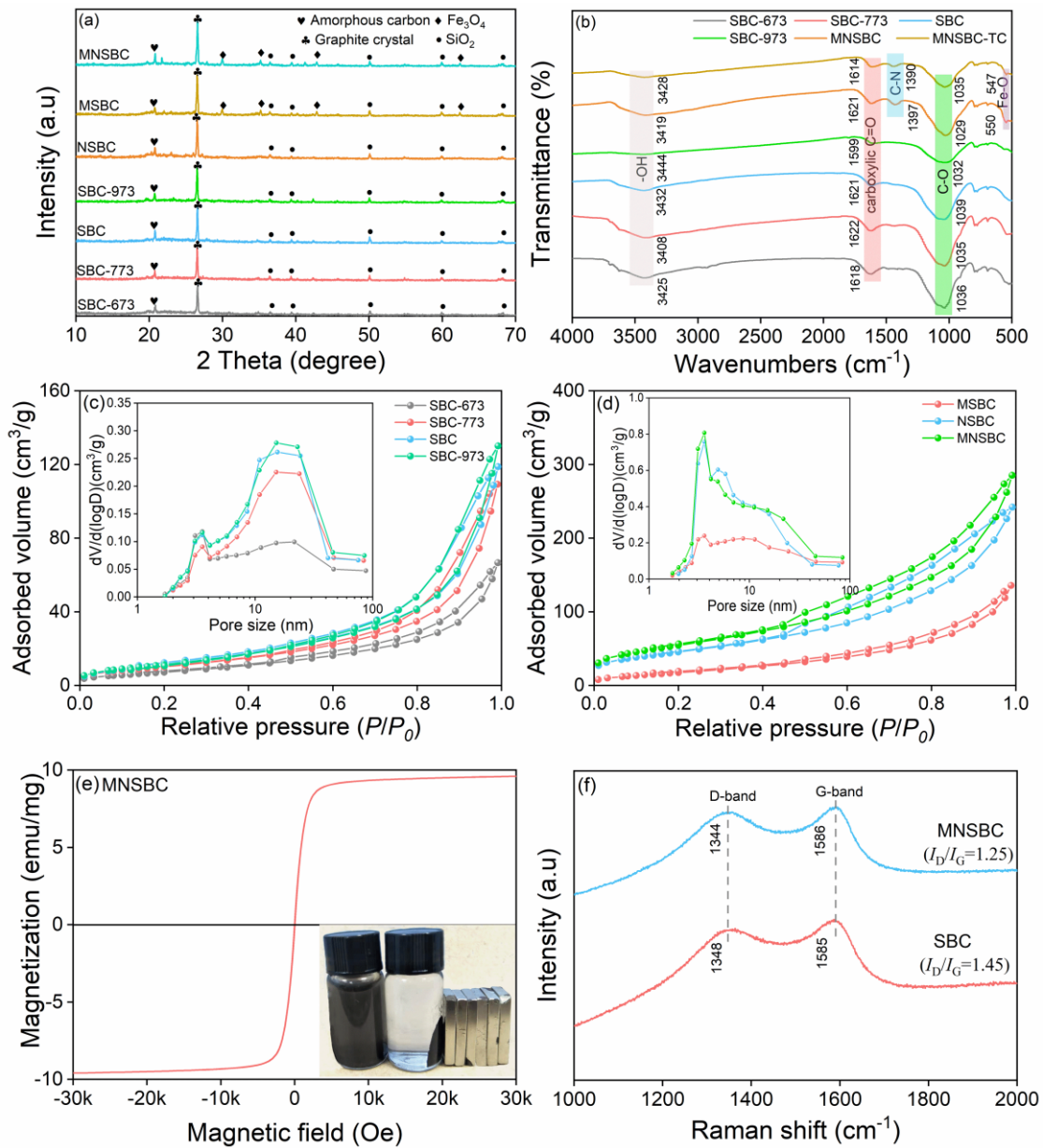
624 [59] P. Liao, Z. Zhan, J. Dai, X. Wu, W. Zhang, K. Wang, S. Yuan, Adsorption of tetracycline and
625 chloramphenicol in aqueous solutions by bamboo charcoal: A batch and fixed-bed column study, *Chem. Eng.*
626 *J.* 228 (2013) 496-505.

627 [60] M. Saood Manzar, T. Ahmad, N. Ullah, P. Velayudhaperumal Chellam, J. John, M. Zubair, R.J. Brandão, L.
628 Meili, O. Alagha, E. Çevik, Comparative adsorption of Eriochrome Black T and Tetracycline by
629 NaOH-modified steel dust: Kinetic and process modeling, *Sep. Purif. Technol.* 287 (2022) 120559.

630

631 **Table 1** Pore structure parameters of SBC-673, SBC-773, SBC, SBC-973, MSBC, NSBC and MNSBC

Biochars	S_{BET} (m ² /g)	V_{tot} (cm ³ /g)	D_p (nm)
SBC-673	44.1	0.115	10.4
SBC-773	60.7	0.187	12.3
SBC	72.5	0.205	11.3
SBC-973	76.5	0.227	11.9
MSBC	113	0.240	8.49
NSBC	231	0.420	7.25
MNSBC	243	0.469	7.72



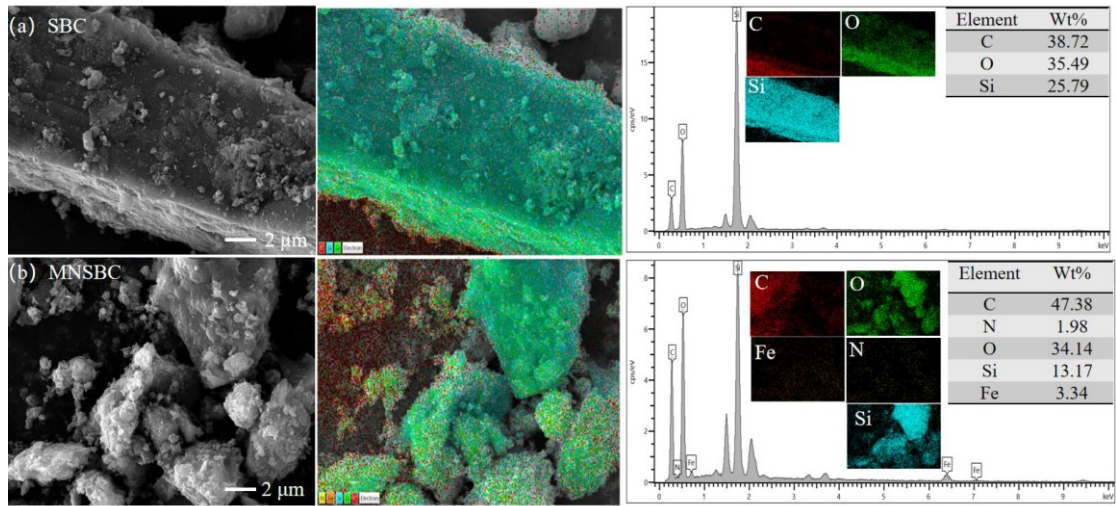
632

633 **Fig. 1.** XRD patterns (a), N_2 adsorption/desorption curves (c) and pore diameter distribution (d) of SBC-673,

634 SBC-773, SBC, SBC-973, MSBC, NSBC and MNSBC; FTIR spectra of SBC-673, SBC-773, SBC, SBC-973,

635 MNSBC and MNSBC-TC (b); magnetic hysteresis loops of MNSBC (e); Raman spectra of SBC and MNSBC (f)

636

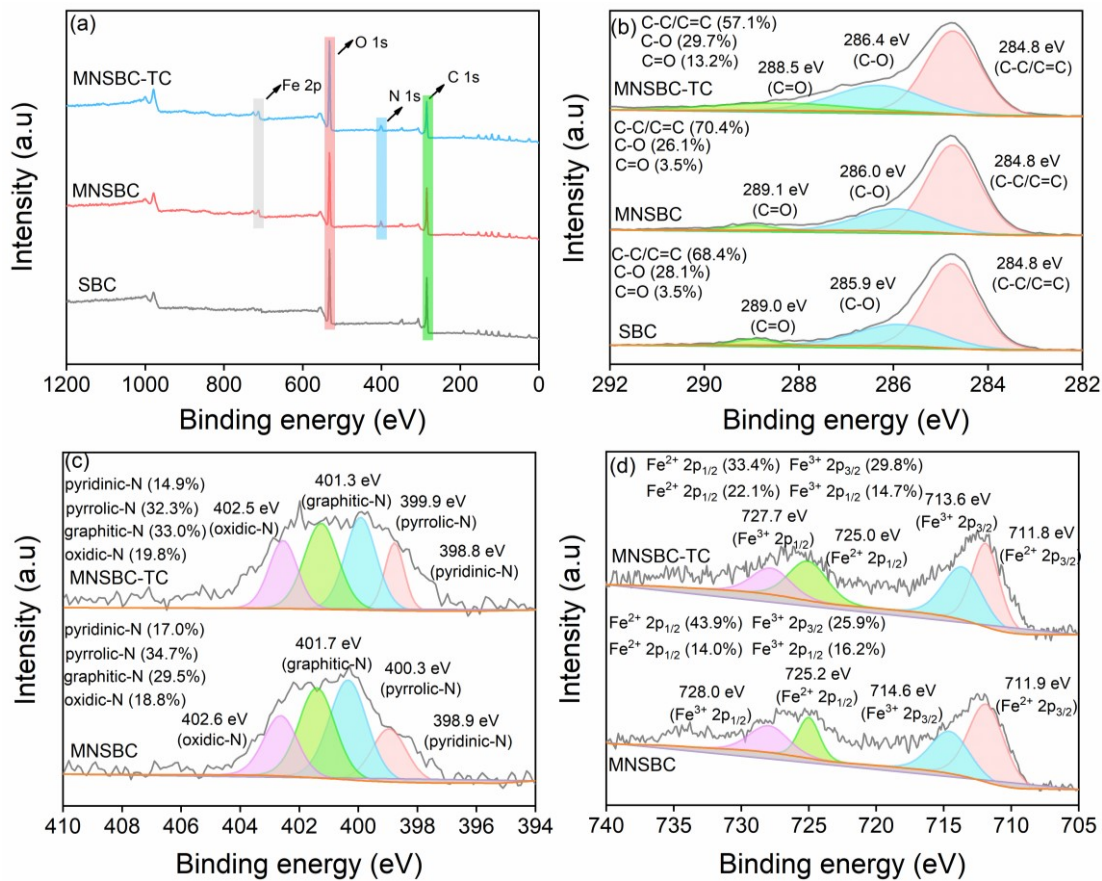


637

638

Fig. 2. The SEM-EDS images of SBC (a) and MNSBC (b)

639



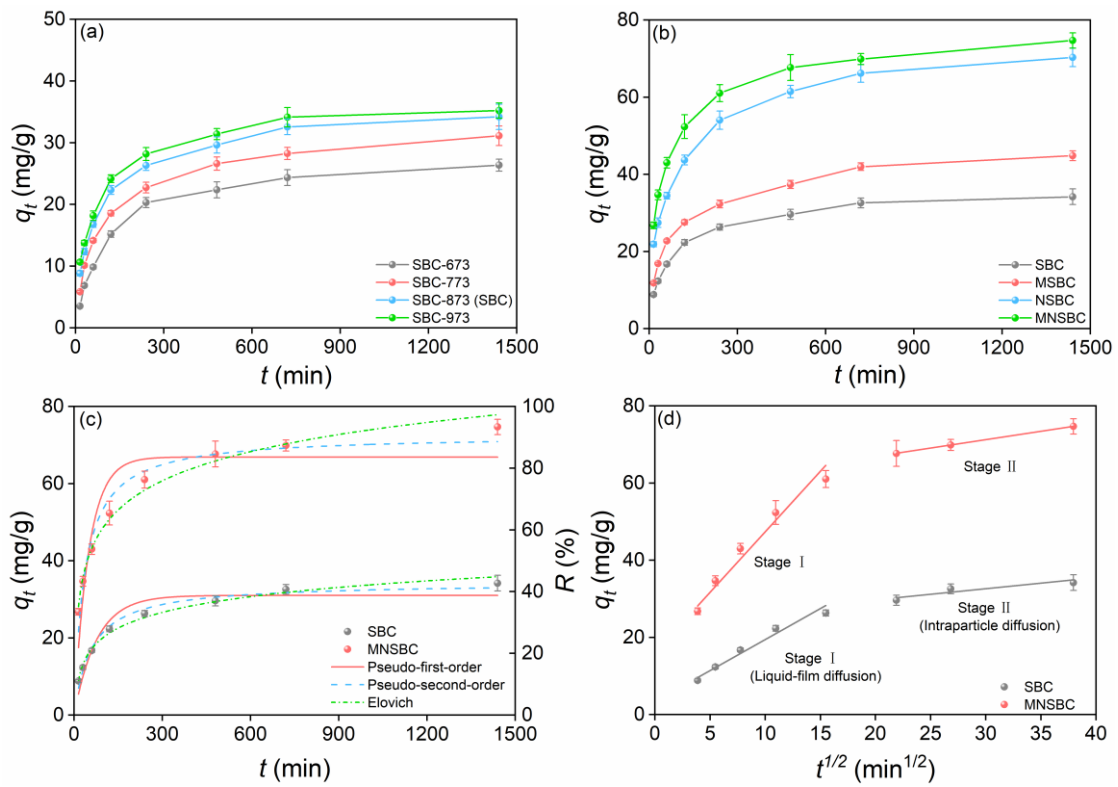
640

641 Fig. 3. XPS survey spectra (a); C 1s of SBC, MNSBC and MNSBC-TC (b); Fe 2p of MNSBC and MNSBC-TC (c);

642

N 1s of MNSBC and MNSBC-TC (d)

643



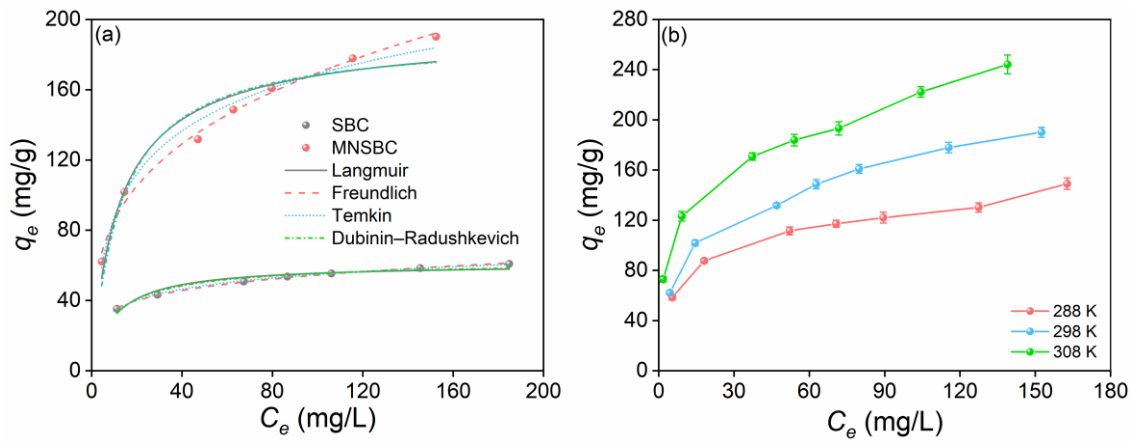
644

645 **Fig. 4.** Effect of pyrolysis temperature on adsorption capacity of SBC for TC (a); adsorption capacity of SBC,

646 MSBC, NSBC and MNSBC for TC (b); kinetics (c) and intraparticle diffusion (d) fitting of TC adsorption onto

647 SBC and MNSBC ($C_0=20$ mg/L, $V=0.1$ L, $m=0.025$ g, $T=298$ K, and $t=0-1440$ min)

648



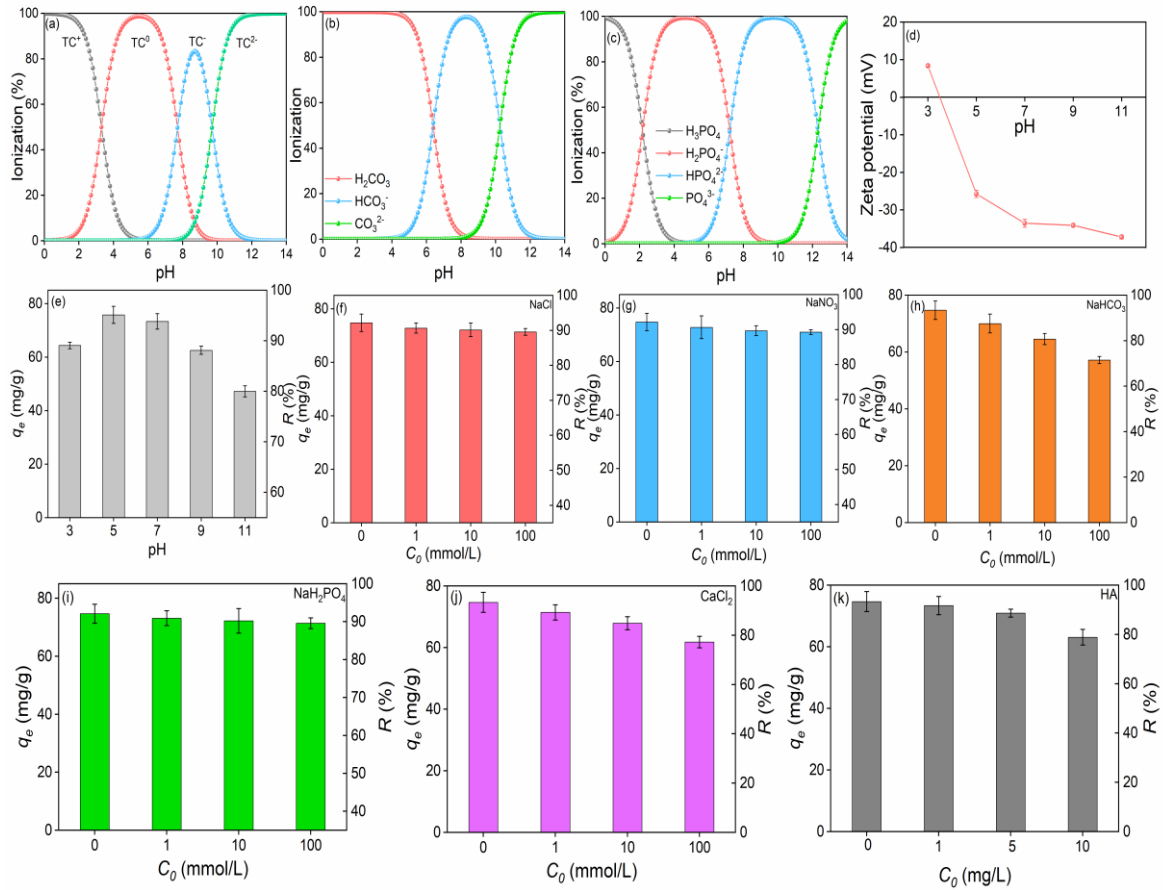
649

650 **Fig. 5.** Isotherms of Langmuir, Freundlich, Temkin and Dubinin–Radushkevich fitting of TC adsorption onto SBC

651 and MNSBC (a); effect of reaction temperature on adsorption capacity of MNSBC for TC (b) (C_0 (TC)=20-200

652 mg/L, $V=0.1$ L, $m=0.025$ g, $T=288-308$ K, and $t=1440$ min)

653



654

655 **Fig. 6.** The species distribution of TC (a), H₂CO₃ (b) and H₃PO₄ (c) at different pH; zeta potential of MNSBC at

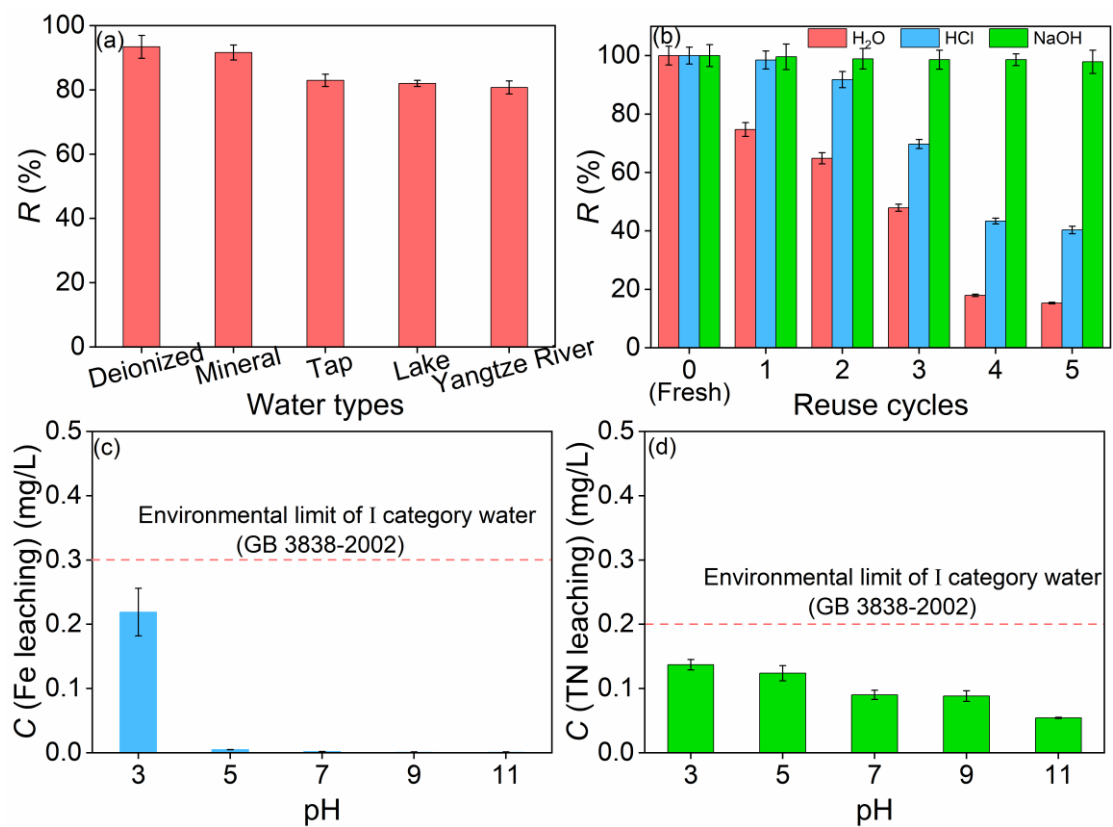
656 different pH (from 3 to 11) (d); effect of pH (from 3 to 11) (e), ionic species/strength (NaCl (f), NaNO₃ (g),

657 NaH₂PO₄ (pH=5) (h), NaHCO₃ (pH=9) (i) and CaCl₂ (j)) and HA concentration (k) on adsorption performance of

658 MNSBC for TC (C_0 (TC)=20 mg/L, $m=0.025$ g, $V=0.1$ L, C_0 (NaCl, NaNO₃, NaH₂PO₄, NaHCO₃ and

659 CaCl₂)=0-100 mmol/L, C_0 (HA)=0-10 mg/L)

660



661

662

Fig. 7. The removal efficiency of MNSBC for TC in various real waters (a); regeneration of MNSBC in reuse

663

cycles by H₂O, HCl and NaOH treatment (b); effect of solution pH on Fe (c) and TN (d) leaching levels of

664

MNSBC (pH=3-11) (C_0 (TC)=20 mg/L, m =0.025 g, V =0.1 L, T =298 K, and t =1440 min)